Title

Strong ferromagnetic exchange interaction under ambient pressure in BaFe2S3

Permalink

https://escholarship.org/uc/item/7tn4d5cw

Journal

Physical Review B, 95(6)

ISSN

2469-9950

Authors

Wang, Meng
Jin, SJ
Yi, Ming
et al.

Publication Date

2017-02-01

DOI

10.1103/physrevb.95.060502

Peer reviewed

Strong ferromagnetic exchange interaction under ambient pressure in BaFe$_2$S$_3$

Meng Wang,[1,2,*] S. J. Jin,[2] Ming Yi,[1] Yu Song,[3] H. C. Jiang,[4] W. L. Zhang,[5] H. L. Sun,[6] H. Q. Luo,[5] A. D. Christianson,[7] E. Bourret-Courchesne,[8] D. H. Lee,[1,8] Dao-Xin Yao,[2] and R. J. Birgeneau[1,8,9]

[1]*Department of Physics, University of California, Berkeley, California 94720, USA*
[2]*School of Physics, Sun Yat-Sen University, Guangzhou 510275, China*
[3]*Department of Physics and Astronomy, Rice University, Houston, Texas 77005, USA*
[4]*Stanford Institute for Materials and Energy Sciences, SLAC National Accelerator Laboratory and Stanford University, Menlo Park, California 94025, USA*
[5]*Beijing National Laboratory for Condensed Matter Physics, Institute of Physics, Chinese Academy of Sciences, Beijing 100190, China*
[6]*Beijing Synchrotron Radiation Facility, Institute of High Energy Physics, Chinese Academy of Science, Beijing 100049, China*
[7]*Quantum Condensed Matter Division, Oak Ridge National Laboratory, Oak Ridge, Tennessee 37831, USA*
[8]*Materials Science Division, Lawrence Berkeley National Laboratory, Berkeley, California 94720, USA*
[9]*Department of Materials Science and Engineering, University of California, Berkeley, California 94720, USA*

Inelastic neutron scattering measurements have been performed to investigate the spin waves of the quasi-one-dimensional antiferromagnetic ladder compound BaFe$_2$S$_3$, where a superconducting transition was observed under pressure [H. Takahashi *et al.*, Nat. Mater. **14**, 1008 (2015); T. Yamauchi *et al.*, Phys. Rev. Lett. **115**, 246402 (2015)]. By fitting the spherically averaged experimental data collected on a powder sample to a Heisenberg Hamiltonian, we find that the one-dimensional antiferromagnetic ladder exhibits a strong nearest-neighbor ferromagnetic exchange interaction ($SJ_R = -71 \pm 4$ meV) along the rung direction, an antiferromagnetic $SJ_L = 49 \pm 3$ meV along the leg direction, and a ferromagnetic $SJ_2 = -15 \pm 2$ meV along the diagonal direction. Our data demonstrate that the antiferromagnetic spin excitations are a common characteristic for the iron-based superconductors, while specific relative values for the exchange interactions do not appear to be unique for the parent states of the superconducting materials.

The mechanism of high-temperature (HTC) superconductivity has been one of the most intensely investigated topics since the discovery of the copper-oxide superconductors [1]. Analogous to the role of phonons in promoting superconductivity in conventional superconductors, spin fluctuations have been viewed as a possible glue that is essential for the formation of Cooper pairs in the HTC superconductors [2,3]. It has been shown that the spin fluctuations in both copper and iron-based superconductors (FeSC) are intimately coupled with the superconductivity, specifically, the appearance of a spin resonance mode in the superconducting (SC) state, and the doping dependence of the spin fluctuations in the normal state [4,5]. The spin fluctuations in a SC compound derive from the spin waves of its magnetically ordered parent compound. Measurements of the spin waves in the parent compound are essential to determine the nature of the spin fluctuations and, in turn, to elucidate their role in the HTC superconductors including the possibility that the spin fluctuations are the primary pairing mechanism.

Recently, a SC transition up to 24 K has been observed in the quasi-one-dimensional (1D) ladder compound BaFe$_2$S$_3$ under pressure in the range of 10 to 17 GPa [8,9]. The obtained pressure-dependent phase diagram [Fig. 1(a)] resembles that of the 1D copper oxide laddered system Sr$_{14-x}$Ca$_x$Cu$_{24}$O$_{41}$ [Fig. 1(b)] [7,10–12] and the commonly observed doping-dependent phase diagrams in the layered FeSC [13]. This suggests that BaFe$_2$S$_3$ at ambient pressure is the parent state of the superconductivity discovered under pressure, and that

the superconductivity likely has a common origin, possibly magnetic-fluctuation-mediated [14]. It has been suggested that the abrupt increase of the Néel temperature (T_N) as a function of pressure shown in Fig. 1(a) is associated with a quantum phase transition due to the change of orbital occupancies under pressure [6]. BaFe$_2$S$_3$ is isostructural with the 1D antiferromagnetic (AF) ladder compounds AFe$_2$Se$_3$ (A = K, Rb, and Cs; space group: $Cmcm$, No. 63) and similar to the slightly distorted material BaFe$_2$Se$_3$ (space group: $Pnma$, No. 62), as shown in Fig. 1(c) [15–22]. The thermal activation gap in BaFe$_2$S$_3$ ($\sim$70 meV) [16] is the smallest among the Fe-based ladder compounds, and photoemission studies suggest that both localized and itinerant $3d$ electrons coexist at room temperature [23]. The FeX (X = Se, S, As, and P) tetrahedra are common among the 1D AF ladder and 2D stripe-ordered materials [24–27]. However, in contrast to the FeX tetrahedra in the other 1D AF ladders [22], the moments of BaFe$_2$S$_3$ are smaller ($\sim$1.2μ_B/Fe) and aligned along the rung direction, as shown in Fig. 1(d) [8], and the distance of the Fe-Fe bonds along the AF direction (leg) is shorter than that along the ferromagnetic (FM) direction (rung). Hence, the spin dynamics, predominantly governed by the geometry of the lattice, could be different in BaFe$_2$S$_3$. Accordingly, it is important to measure the spin waves of BaFe$_2$S$_3$ and extract the exchange interactions in order to compare with the other 1D and 2D analogs.

In this Rapid Communication, we report inelastic neutron scattering (INS) studies on the spin waves of a BaFe$_2$S$_3$ powder sample. Similarly to our measurements on RbFe$_2$Se$_3$ [22], we observe an acoustic branch and an optical branch of spin waves, consistent with two inequivalent iron sites in
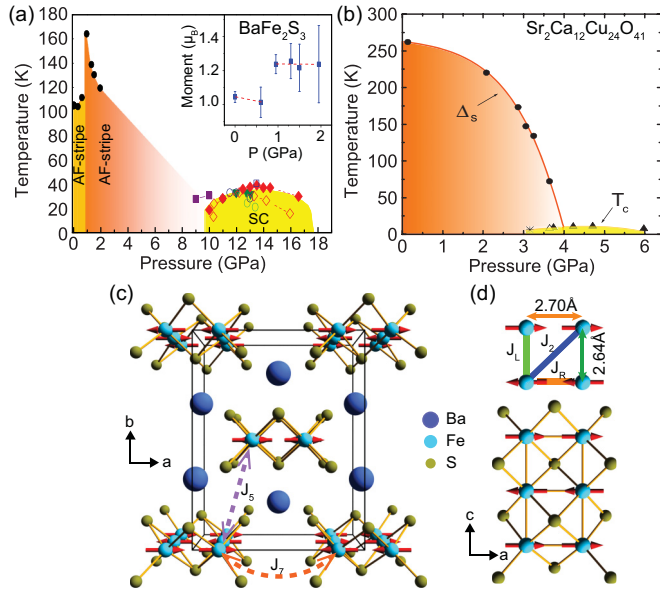
*wangmeng5@mail.sysu.edu.cn

FIG. 1. (a) Pressure dependence of the AF and superconducting transitions, and the moment sizes (inset panel) for $BaFe_2S_3$ adopted from Ref. [6]. (b) Pressure dependence of the spin gap (Δ_s) and superconducting transitions for the laddered compound $Sr_2Ca_{12}Cu_{24}O_{41}$ adopted from Ref. [7]. (c) A sketch of the ladder structure of $BaFe_2S_3$. The cuboid indicates one unit cell. (d) One-dimensional edge-shared FeS tetrahedra in $BaFe_2S_3$. The red arrows represent the moment directions of irons. The J_L, J_R, J_2, J_5, and J_7 are the magnetic exchange interactions between the corresponding irons.

the magnetic unit cell. From the spherically averaged spectra on the powder sample, we are able to extract a spin gap, two band tops of the acoustic branch along two directions, and the minimum and maximum energies of the optical branch. By solving the Heisenberg Hamiltonian of the ladder structure with the observed constraints, we determine a set of parameters ($SJ_R = -71 \pm 4, SJ_L = 49 \pm 3, SJ_2 = -15 \pm 2, SJ_7 = 3.0 \pm 0.5$, and $SJ_s = 0.1 \pm 0.04$ meV) with a strong intraladder FM exchange interaction along the rung direction that fits the experimental data well. The results demonstrate that the spin fluctuations are comparable among various parent compounds of the FeSC, while the exchange interactions that are previously proven universal are not unique for the stripe AF ordered parent state of the FeSC.

The $BaFe_2S_3$ samples were grown using the Bridgman method [27]; they formed in small needle-like single crystals, making them extremely difficult to align. Hence we ground 8 g of the single crystals into a powder for this experiment. Our INS experiment was carried out on the ARCS time-of-flight chopper spectrometer [28] at the Spallation Neutron Source, Oak Ridge National laboratory (SNS, ORNL). The powder sample was sealed in an aluminum can and loaded into a He top-loading refrigerator. The sample was measured with incident beam energies of $E_i = 50, 150$, and 250 meV at 5 K. The energy resolutions for these incident beams were $\Delta E = 2.2, 7.0$, and 13.3 meV, as determined by the full width at half maximum (FWHM) of the energy cuts at $E = 0$ meV. The SpinW program [29] that employs classical Monte Carlo simulations and linear spin wave theory is used for simulations and comparisons with experimental data.

Figure 2 shows INS spectra and cuts for the $BaFe_2S_3$ powder samples with different incident energies. In Fig. 2(a), we can see intense excitations at $Q = 1.27$ Å^{-1}, dispersive excitations stemming from $Q = 2.19$ and 2.81 Å^{-1}, weak excitations at $Q = 3.59$ Å^{-1}, and a gap around 5 meV for all the Qs. The spectrum resembles the spin waves observed on the ladder compound $RbFe_2Se_3$ [22]. The four Qs are consistent with the AF wave vectors at $(H,K,L) = (0.5,0.5,1),(2.5,0.5,1),(3.5,0.5,1)$, and $(0.5,0.5,3)$, revealing that the excitations are the spin waves of $BaFe_2S_3$. Here, (H,K,L) are Miller indices for the momentum transfer $|Q| = 2\pi\sqrt{(H/a)^2 + (K/b)^2 + (L/c)^2}$, where the lattice constants are $a = 8.79, b = 11.23$, and $c = 5.29$ Å [8]. The flat excitations with intensities increasing with Q below 30 meV are phonons associated with the sample and the thin aluminum can.

To determine the spin gap and dispersion relations quantitatively, we present a constant Q cut integrated within $Q = 1.27 \pm 0.1$ Å^{-1} in Fig. 2(e) and constant energy cuts within $E = 6 \pm 1, 12 \pm 1, 18 \pm 1, 24 \pm 1$, and 30 ± 1 meV in Fig. 2(f). The minimum of the in-ladder plane and out-of-ladder plane spin gaps is 5 ± 1 meV [44]. The spin excitations stemming from $Q = 2.19$ and 2.81 Å^{-1} disperse separately into four peaks with increasing energy. At around 30 meV, the two inner peaks merge together, indicating that the spin waves have reached a maximum along the $[H,0.5,1]$ direction. Figures 2(b) and 2(g) present the dispersive spin excitations at $Q = 3.59$ Å^{-1} with $E_i = 80$ meV. The spin excitations continuously evolve into dispersionless excitations at 70 meV, as shown in Figs. 2(c) and 2(h). This energy (~70 meV) is higher than the cutoff energy of phonons and the intensities decrease with increasing Q, indicating that they are magnetic excitations of $BaFe_2S_3$. The dispersion relation at $Q = (0.5,0.5,3) = 3.59$ Å^{-1} corresponds to the dispersion along the $[0.5,0.5,L]$ direction. Thus, the dispersionless spin excitations at 70 meV can be ascribed to the zone boundary excitations along the L direction. Gaussian peak fittings to the constant Q cuts of the dispersionless spin excitations in Fig. 2(h) show centers at $71 \sim 72$ meV. The energy is significantly lower than the observed spin wave maximum (~190 meV) along the same direction for $RbFe_2Se_3$ [22].

In Fig. 2(d), we present the optical spin waves measured with $E_i = 250$ meV at 5 K. Two flat branches of excitations are observed. The center of the lower branch is determined to be at 171.6 ± 0.3 meV within $Q = 5.75 \pm 0.25$ Å^{-1} and 176 ± 2 meV within $Q = 7.75 \pm 0.25$ Å^{-1}, and that of the higher branch is at 210.7 ± 0.3 meV within $Q = 7.75 \pm 0.25$ Å^{-1}. The low and high branches of magnetic excitations are consistent with them being the minimum and maximum of the optical branch of the spin waves of $BaFe_2S_3$. The extracted spin wave dispersion relations have been plotted in Fig. 3.

$BaFe_2S_3$ at ambient pressure exhibits a stripe-ordered structure similar to that of $RbFe_2Se_3$ [22]. We proceed to employ the simple bilinear Heisenberg Hamiltonian that has been used to successfully describe the spin waves of the ladder compound $RbFe_2Se_3$ and other 2D stripe systems to fit the dispersion relations and extract the magnetic exchange interactions for $BaFe_2S_3$ [22,30–34]. The spin Hamiltonian is
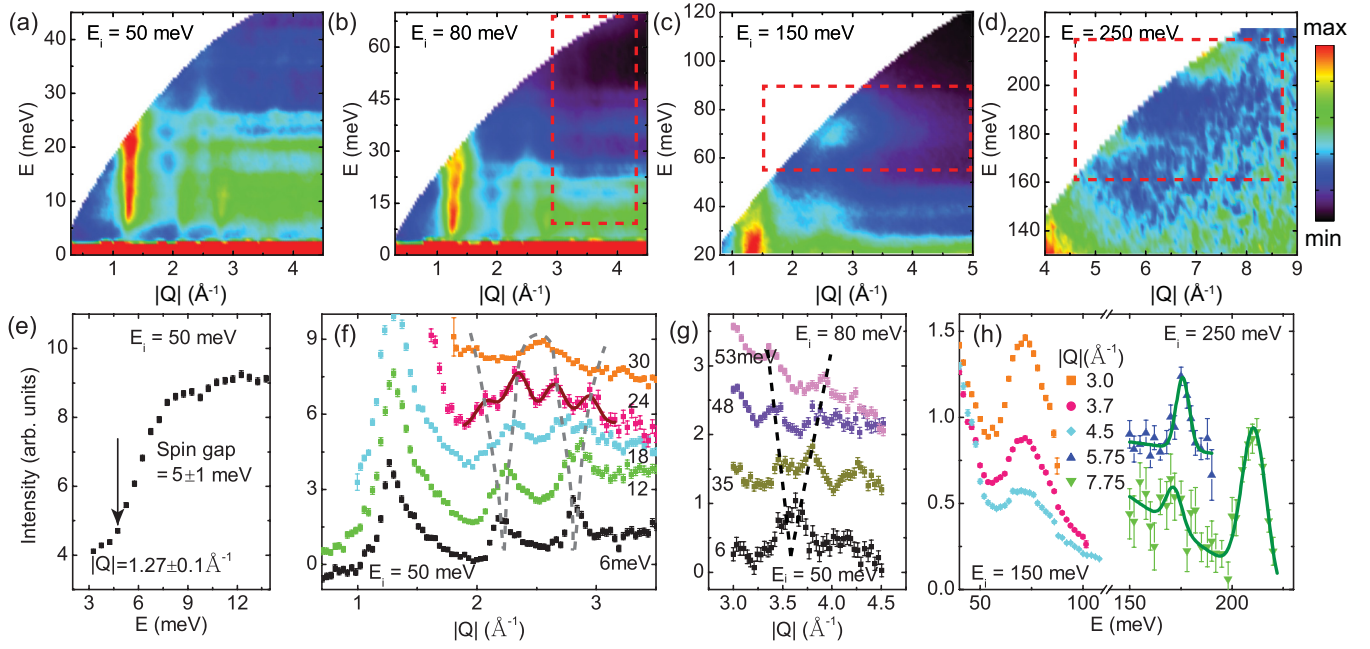
FIG. 2. (a) INS spectra $S(Q,\omega)$ of $BaFe_2S_3$ at 5 K with $E_i = 50$, (b) 80, (c) 150, and (d) 250 meV. The color represents intensities in arbitrary units. The red dashed rectangles highlight the areas for the cuts in (g) and (h). (e) Constant Q cut with $E_i = 50$ meV between $1.26 < Q < 1.28$ Å^{-1}. (f) Constant energy cuts at $E = 6, 12, 18, 24$, and 30 meV integrated within $E \pm 1$ meV with $E_i = 50$ meV. (g) Similar constant energy cuts at $E = 6 \pm 1, 35 \pm 1$ meV with $E_i = 50$ meV and $E = 48 \pm 1.5, 53 \pm 1.5$ meV with $E_i = 80$ meV at 5 K. The dashed lines are guides to the dispersion relations of spin excitations. The solid line on top of $E = 24$ meV data points is a fit to Gaussian functions. The intensities for $E = 24$ meV in (f) and 48 and 53 meV in (g) have been doubled for comparison. (h) Constant Q cuts at $Q = 3.0, 3.7, 4.5$ Å^{-1} integrated within $Q \pm 0.15$ Å^{-1} with $E_i = 150$ meV and $Q = 5.75, 7.75$ Å^{-1} integrated within $Q \pm 0.25$ Å^{-1} with $E_i = 250$ meV. The green solid lines are fits to Gaussian functions. The error bars are one standard deviation of the measured counts.

written as

$$\hat{H} = \sum_{r,r'} \frac{J_{r,r'}}{2} \mathbf{S}_r \cdot \mathbf{S}_{r'} - J_s \sum_r (\mathbf{S}_r^z)^2, \quad (1)$$

where $J_{r,r'}$ are the effective exchange couplings and (r,r') label the iron sites; J_s is the single ion Ising anisotropy term [35]. By solving Eq. (1) using the linear spin wave approximation, the dispersion relations and extrema values can be obtained [35]. Because we have assumed identical Hamiltonians for the spin waves of $BaFe_2S_3$ and $RbFe_2Se_3$, the solutions have the same analytical expressions [22]. The spin gap Δ_s, the tops of the acoustic mode along the H direction (E_{1t}^H) and L direction (E_{1t}^L), and the bottom (E_{2b}) and top (E_{2t}) of the optical mode are as follows:

$$\Delta_s = 2S\sqrt{J_s(2J_L + 2J_2 + J_7 + J_s)},$$

$$E_{1t}^H = 2S\sqrt{(2J_L + 2J_2 + J_s)(J_7 + J_s)},$$

$$E_{1t}^L = 2S\sqrt{(J_L + J_2 + J_s)(J_L + J_2 + J_7 + J_s)},$$

$$E_{2b} = 2S\sqrt{(2J_L - J_R + J_s)(2J_2 - J_R + J_7 + J_s)},$$

$$E_{2t} = 2S\sqrt{(J_L - J_R + J_2 + J_s)(J_L - J_R + J_2 + J_7 + J_s)}.$$

$$\qquad\qquad\qquad (2)$$

The J_R, J_L, and J_2 are the intraladder exchange interactions along the rung, leg, and diagonal directions, respectively. J_7 is the seventh-nearest-neighbor (NN) exchange interaction of irons between two ladders, as defined in Fig. 1(c). The expressions in Eq. (2) correspond to the wave vectors at

$Q = (H,L) = (0.5,1),(1,1),(0.5,0.5),(1,1)$, and $(1,0.5)$, respectively. The K for these wave vectors is 0.5.

From the spherically averaged INS data, we have determined the values for these extrema, where $\Delta_s \approx 5, E_{1t}^H \approx 30$, $E_{1t}^L \approx 72, E_{2b} \approx 172$, and $E_{2t} \approx 211$ meV. Solving Eq. (2) would lead to two sets of mathematical solutions. By comparing with the experimental data, the two sets of parameters are determined as $SJ_L = 49.3, SJ_2 = -15.1$ meV and $SJ_L = -14.3, SJ_2 = 48.4$ meV, respectively, while the other interactions, $SJ_R = -70.5, SJ_7 = 3.0$, and $SJ_s = 0.1$ meV, are the same. The two sets of parameters fit our spherically averaged data equally well. However, there is a difference for the optical spin wave branch for single crystals [44]. The intensity distribution of the optical mode for the second set of parameters disagrees with that of $RbFe_2Se_3$, where the intensities at $(H,L) = (1,1)$ are stronger than that at $(1,0)$ [22]. The FM J_L is also contrary to a first-principles calculation [36], which predicts an AF J_L and a FM J_R. Furthermore, the inferred $SJ_2 = 48.4$ meV is much larger than the expectation for a superexchange interaction between two irons with the distance of 3.78 Å [22,34]. Thus, the second set of parameters is unlikely to be a physical solution for the Hamiltonian for the spin waves of $BaFe_2S_3$.

We hence determine the products of the spin S and exchange interactions as $SJ_R = -71 \pm 4, SJ_L = 49 \pm 3, SJ_2 = -15 \pm 2$, $SJ_7 = 3.0 \pm 0.5$, and $SJ_s = 0.1 \pm 0.04$ meV for $BaFe_2S_3$. The errors are estimated by considering the effects on the spin wave extrema in Eq. (2). There should be other weak out-of-ladder plane exchange couplings, e.g., J_5, that give rise
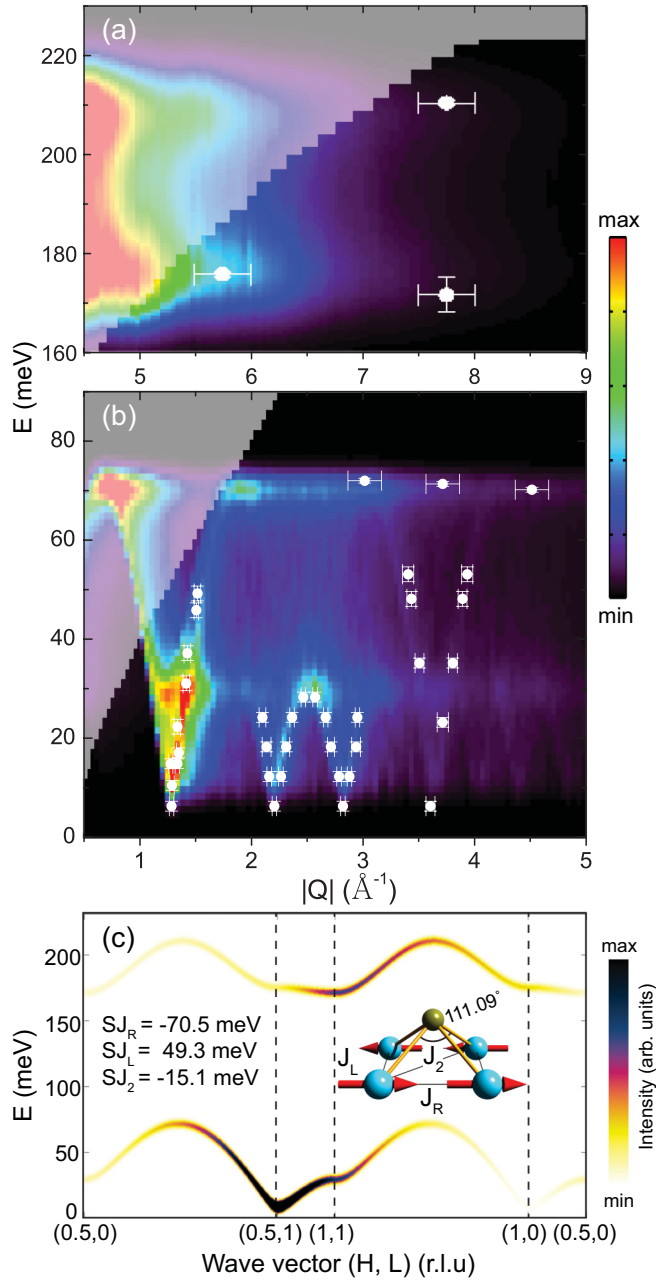
FIG. 3. Comparisons between the SpinW simulated spin excitation spectra and experimentally determined dispersion relations (white points) for $BaFe_2S_3$. (a) Instrumental resolutions of 13.3 meV and (b) 5 meV have been convolved for comparison with the powder-averaged experimental data in Figs. 2(a)–2(d). The white shaded areas are experimentally inaccessible with $E_i = 250$ meV. (c) SpinW simulated spin excitations along high-symmetry directions in the $[H, L]$ 2D Brillouin zone for single crystals with the parameters labeled on the figures. The other parameters, SJ_7 and SJ_s, have been fixed at 3.0 and 0.1 meV, respectively. The color represents intensities. We convolve a constant 5 meV instrumental resolution for visualization. The inset in panel (c) shows a tetrahedron and associated exchange interactions.

to the three-dimensional magnetic order, as shown in Fig. 1(a). However, we could not determine them from the spherically averaged powder data. The SpinW simulated spherically

averaged spectra based on the determined exchange interactions together with the dispersion relations extracted from our experimental data and the spin wave spectrum for single crystals are plotted in Fig. 3. The simulated spectra match the experimental data well.

We list the anisotropic SJ's and NN Fe-Fe bond lengths for the stripe-ordered $S \approx 1/2$ "122" compounds, $S \approx 2$ "234" compound, and iron-ladder "123" compounds in Table I for comparison. A set of isotropic $J_{AF} = J_F$ with a large biquadratic term might be able to fit the data [37,38]. However, a biquadratic model cannot reasonably explain the universality of the SJ's observed in materials for S varying from 1/2 to 2. The magnitude of the AF SJ_L for $BaFe_2S_3$ is comparable with the SJ_{AF} along the AF-ordered direction for the other 1D and 2D analogs [22,30–33]. However, the strong FM J_R and FM J_2 are distinguishable. Following the Goodenough-Kanamori rules [39,40], a superexchange interaction (J_2) connects d orbitals of two magnetic atoms (M) via p orbitals of the atom (X) in between. For the case of an M-X-M angle $\alpha = 180°$, both the d orbitals couple to the same p orbital, resulting in an AF J_2. However, for the angle $\alpha = 90°$, the d orbitals couple to two orthogonal p orbitals, making it impossible for an electron on one d orbital to reach the d orbital on the other site. In this case, the superexchange mediated via the Coulomb exchange on the connected two orthogonal p orbitals is expected to be ferromagnetic. In $BaFe_2S_3$, the angle of the Fe-S-Fe along the diagonal direction is $111.09°$. The competition between the AF and FM superexchange processes could give rise to a FM J_2. The extracted FM J_2 and the strong FM J_R in $BaFe_2S_3$ could be ascribed to this unique geometry, where the bonds along the AF-ordered direction (d_{AF}) are shorter than that along the FM-ordered direction (d_F), as shown in Table I. The diagonal direction always leans towards the stronger NN exchange (J_1) direction and J_2 also exhibits the same sign as J_1. The J_2 could be dominated by the closer J_1 in the stripe-AF-ordered Fe-based materials. On the other hand, the presence of a possible small biquadratic exchange interaction could also account for the effective FM J_2 [41]. Interestingly, a direct fitting with the J_1-J_2 model to the spin waves of La_2CuO_4 also results in a FM J_2, which has been ascribed by the authors to the effect of a cyclic or ring exchange interaction [42].

The ratio of the exchange interactions has been suggested to be crucial for the SC pairing symmetry and even whether or not superconductivity occurs in the FeSC [43]. A possible orbital ordering transition near 200 K merges gradually together

TABLE I. The magnetic exchange couplings and NN Fe-Fe distances along the antiferromagnetic (J_{AF} and d_{AF}) and ferromagnetic (J_F and d_F) directions, respectively, and the exchange couplings along the diagonal direction for various Fe-based materials [22,30–33]. The bond distances, d_{AF} and d_F, are in angstrom units (Å).

Compounds	SJ_{AF}	SJ_F	SJ_2 (meV)	d_{AF}	d_F
$CaFe_2As_2$	50 ± 10	-6 ± 5	19 ± 4	2.753	>2.703
$BaFe_2As_2$	59 ± 2	-9 ± 2	14 ± 1	2.808	>2.786
$SrFe_2As_2$	39 ± 2	-5 ± 5	27 ± 1	2.785	>2.756
$Rb_2Fe_3S_4$	42 ± 5	-20 ± 2	17 ± 2	2.76	>2.70
$RbFe_2Se_3$	70 ± 5	-12 ± 2	25 ± 5	2.77	>2.64
$BaFe_2S_3$	49 ± 3	-71 ± 4	-15 ± 1	2.64	<2.70

with the magnetic ordering transition ($\sim$120 K) at 2 GPa, accompanying the abrupt increases of T_N and the moment sizes at 1 GPa [6,9]. Superconductivity emerges around 10 GPa, where the magnetic order has been suppressed [8,9]. Clearly, the orbital ordering, magnetism, and superconductivity are strongly coupled and all of them are sensitive to pressure. The exchange interactions we extract from $BaFe_2S_3$ should be related to its unique FeS tetrahedra. Our results clearly are important for any theoretical modeling of the superconductivity based on the spin-fluctuation-mediated mechanism and for any theoretical investigation of the interplay between the magnetic ordering, orbital ordering, and superconductivity.

In summary, we have measured the spin wave spectra of the stripe AF order in the 1D ladder compound $BaFe_2S_3$ on a powder sample. Guided by the analytical expressions for the extrema of the spin waves and their experimentally determined values, the Heisenberg exchange interactions have been successfully determined. Spherically averaged simulations using the parameters so determined match well the measured spectra. The explicit values for the exchange interactions in $BaFe_2S_3$ are distinct from those of the other 1D and 2D analogs due to its unique structural geometry. The results reveal that the 1D AF-ordered ladder parent state of the superconductivity in $BaFe_2S_3$ exhibits the commonly observed antiferromagnetic spin excitations just as in the parent compounds of the other FeSC. However, there are important quantitative differences from the previously realized combinations of exchange interactions for the stripe-AF-ordered parent state of the FeSC, suggesting that a wider range of interactions may still result in superconductivity.

[1] Q. Si, R. Yu, and E. Abrahams, Nat. Rev. Mater. **1**, 16017 (2016).

[2] J. Bardeen, L. N. Cooper, and J. R. Schrieffer, Phys. Rev. **108**, 1175 (1957).

[3] D. J. Scalapino, Rev. Mod. Phys. **84**, 1383 (2012).

[4] P. Dai, Rev. Mod. Phys. **87**, 855 (2015).

[5] M. Wang, C. L. Zhang, X. Y. Lu, G. T. Tan, H. Q. Luo, Y. Song, M. Y. Wang, X. T. Zhang, E. A. Goremychkin, T. G. Perring, T. A. Maier, Z. P. Yin, K. Haule, G. Kotliar, and P. C. Dai, Nat. Commun. **4**, 2874 (2013).

[6] S. Chi, Y. Uwatoko, H. Cao, Y. Hirata, K. Hashizume, T. Aoyama, and K. Ohgushi, Phys. Rev. Lett. **117**, 047003 (2016).

[7] Y. Piskunov, D. Jérome, P. Auban-Senzier, P. Wzietek, C. Bourbonnais, U. Ammerhal, G. Dhalenne, and A. Revcolevschi, Eur. Phys. J. B **24**, 443 (2001).

[8] H. Takahashi, A. Sugimoto, Y. Nambu, T. Yamauchi, Y. Hirata, T. Kawakami, M. Avdeev, K. Matsubayashi, F. Du, C. Kawashima *et al.*, Nat. Mater. **14**, 1008 (2015).

[9] T. Yamauchi, Y. Hirata, Y. Ueda, and K. Ohgushi, Phys. Rev. Lett. **115**, 246402 (2015).

[10] M. Uehara and T. Nagata, J. Phys. Soc. Jpn. **65**, 2764 (1996).

[11] T. Nagata, H. Fujino, J. Akimitsu, M. Nishi, K. Kakurai, S. Katano, M. Hiroi, M. Sera, and N. Kobayashi, J. Phys. Soc. Jpn. **68**, 2206 (1999).

[12] T. Vuletić, B. Korin-Hamzić, T. Ivek, S. Tomić, B. Gorshunov, M. Dressel, and J. Akimitsu, Phys. Rep. **428**, 169 (2006).

[13] G. R. Stewart, Rev. Mod. Phys. **83**, 1589 (2011).

[14] R. Arita, H. Ikeda, S. Sakai, and M.-T. Suzuki, Phys. Rev. B **92**, 054515 (2015).

[15] H. Hong and H. Steinfink, J. Solid State Chem. **5**, 93 (1972).

[16] W. M. Reiff, J. Solid State Chem. **13**, 32 (1975).

[17] K. Klepp, W. Sparlinek, and H. Boller, J. Alloys Compd. **238**, 1 (1996).

[18] B. Saparov, S. Calder, B. Sipos, H. Cao, S. Chi, D. J. Singh, A. D. Christianson, M. D. Lumsden, and A. S. Sefat, Phys. Rev. B **84**, 245132 (2011).

[19] F. Du, K. Ohgushi, Y. Nambu, T. Kawakami, M. Avdeev, Y. Hirata, Y. Watanabe, T. J. Sato, and Y. Ueda, Phys. Rev. B **85**, 214436 (2012).

[20] J. M. Caron, J. R. Neilson, D. C. Miller, K. Arpino, A. Llobet, and T. M. McQueen, Phys. Rev. B **85**, 180405(R) (2012).

[21] Y. Nambu, K. Ohgushi, S. Suzuki, F. Du, M. Avdeev, Y. Uwatoko, K. Munakata, H. Fukazawa, S. Chi, Y. Ueda *et al.*, Phys. Rev. B **85**, 064413 (2012).

[22] M. Wang, M. Yi, S. Jin, H. C. Jiang, Y. Song, H. Luo, A. D. Christianson, C. D. Cruz, D.-X. Yao, D. H. Lee *et al.*, Phys. Rev. B **94**, 041111 (2016).

[23] D. Ootsuki, N. L. Saini, F. Du, Y. Hirata, K. Ohgushi, Y. Ueda, and T. Mizokawa, Phys. Rev. B **91**, 014505 (2015).

[24] J. W. Lynn and P. Dai, Physica C **469**, 469 (2009).

[25] Q. Huang, Y. Qiu, W. Bao, M. A. Green, J. W. Lynn, Y. C. Gasparovic, T. Wu, G. Wu, and X. H. Chen, Phys. Rev. Lett. **101**, 257003 (2008).

[26] J. Zhao, H. Cao, E. Bourret-Courchesne, D. H. Lee, and R. J. Birgeneau, Phys. Rev. Lett. **109**, 267003 (2012).

[27] M. Wang, W. Tian, P. Valdivia, S. Chi, E. Bourret-Courchesne, P. Dai, and R. J. Birgeneau, Phys. Rev. B **90**, 125148 (2014).

[28] D. L. Abernathy, M. B. Stone, M. J. Loguillo, M. S. Lucas, O. Delaire, X. Tang, J. Y. Y. Lin, and B. Fultz, Rev. Sci. Instrum. **83**, 015114 (2012).

[29] S. Toth and B. Lake, J. Phys.: Condens. Matter **27**, 166002 (2015).

[30] J. Zhao, D. T. Adroja, D.-X. Yao, R. Bewley, S. Li, X. F. Wang, G. Wu, X. H. Chen, J. Hu, and P. Dai, Nat. Phys. **5**, 555 (2009).

[31] R. A. Ewings, T. G. Perring, J. Gillett, S. D. Das, S. E. Sebastian, A. E. Taylor, T. Guidi, and A. T. Boothroyd, Phys. Rev. B **83**, 214519 (2011).

[32] L. W. Harriger, H. Q. Luo, M. S. Liu, C. Frost, J. P. Hu, M. R. Norman, and P. Dai, Phys. Rev. B **84**, 054544 (2011).

[33] M. Wang, P. Valdivia, M. Yi, J. X. Chen, W. L. Zhang, R. A. Ewings, T. G. Perring, Y. Zhao, L. W. Harriger, J. W. Lynn *et al.*, Phys. Rev. B **92**, 041109(R) (2015).

[34] J. Zhao, Y. Shen, R. J. Birgeneau, M. Gao, Z. Y. Lu, D. H. Lee, X. Z. Lu, H. J. Xiang, D. L. Abernathy, and Y. Zhao, Phys. Rev. Lett. **112**, 177002 (2014).

[35] D. X. Yao and E. W. Carlson, Front. Phys. China **5**, 166 (2010).

[36] M.-T. Suzuki, R. Arita, and H. Ikeda, Phys. Rev. B **92**, 085116 (2015).

[37] S. O. Diallo, V. P. Antropov, T. G. Perring, C. Broholm, J. J. Pulikkotil, N. Ni, S. L. Bud'ko, P. C. Canfield, A. Kreyssig, A. I. Goldman *et al.*, Phys. Rev. Lett. **102**, 187206 (2009).

[38] A. L. Wysocki, K. D. Belashchenko, and V. P. Antropov, Nat. Phys. **7**, 485 (2011).

[39] G. J. B., Scholarpedia **3**, 7382 (2008).

[40] E. Pavarini, E. Koch, F. Anders, and M. Jarrell, *Correlated Electrons: From Models to Materials Modeling and Simulation*, Vol. 2 (Forschungszentrum Jülich, 2012).

[41] C. Luo, T. Datta, and D.-x. Yao, Phys. Rev. B **93**, 235148 (2016).

[42] R. Coldea, S. M. Hayden, G. Aeppli, T. G. Perring, C. D. Frost, T. E. Mason, S. W. Cheong, and Z. Fisk, Phys. Rev. Lett. **86**, 5377 (2001).

[43] F. Yang, F. Wang, and D. H. Lee, Phys. Rev. B **88**, 100504(R) (2013).

[44] See Supplemental Material at http://link.aps.org/supplemental/10.1103/PhysRevB.95.060502 for DMRG calculations for the quantum mechanical spin gap and simulated spin wave spectra for single crystals with two sets of parameters.